Catalysis Science & Technology

ROYAL SOCIETY OF CHEMISTRY

PAPER

View Article Online
View Journal

Cite this: DOI: 10.1039/d1cy00109d

Design and characterization of novel dirhodium coordination polymers – the impact of ligand size on selectivity in asymmetric cyclopropanation†

Zhenzhong Li,[a] Lorenz Rösler,[a] Till Wissel,[a] Hergen Breitzke,[a] Kathrin Hofmann,[a] Hans-Heinrich Limbach,[b] Torsten Gutmann *[a] and Gerd Buntkowsky *[a]

Received 20th January 2021,
Accepted 14th March 2021

DOI: 10.1039/d1cy00109d

rsc.li/catalysis

Three chiral dirhodium coordination polymers Rh_2–L*n* (*n* = 1–3) have been synthesized *via* ligand exchange between dirhodium trifluoroacetate $Rh_2(TFA)_4$ and differently sized chiral dicarboxylic acids derived from L-*tert*-leucine. SEM images indicate that the Rh_2–L*n* (*n* = 1–3) polymers have a lamellar structure. XPS data demonstrate that the oxidation state of rhodium in the dirhodium nodes is maintained during the synthesis of the polymers. The coordination polymers have been further characterized by FTIR, $^1H \rightarrow {}^{13}C$ CP MAS NMR and ^{19}F MAS NMR spectroscopy to prove the formation of polymers *via* ligand exchange. Although the quantitative ^{19}F MAS NMR spectra reveal incomplete ligand substitution in the coordination polymers, these catalysts show excellent activity and selectivity in the asymmetric cyclopropanation reaction between styrene and diazooxindole. In particular, the enantioselectivity has been significantly improved compared with previously designed dirhodium coordination polymers, which were synthesized from aromatic dicarboxylic acids derived from L-phenylalanine. Meanwhile, the dirhodium polymers can be easily recycled five times without significant reduction in their catalytic efficiency.

Introduction

Homogeneous transition-metal catalysts are widely used for the industrial scale production of fine chemicals, pharmaceuticals and molecular organic materials owing to their high activity and selectivity.[1,2] However, their recovery and recycling is often challenging. This inevitably adds costs especially to avoid metal contamination of pharmaceuticals.[3–5] Accordingly, the development of heterogeneous organometallic catalysts is considered to be an effective way to overcome these intrinsic problems of homogeneous catalysts.[6] However, heterogeneous catalysts usually show inferior catalytic performances compared to their homogeneous counterparts. This observation mainly refers to the mass transfer limitation induced by solid carrier materials, and to the change of the chemical environment of active sites during the multistep preparation of heterogeneous catalysts.[7,8] Therefore, further development of a facile and efficient approach for the fabrication of heterogeneous transition metal catalysts with high catalytic performance is urgently needed.

Chiral dirhodium(II) complexes are important examples of organometallic catalysts. They have drawn much attention due to their unique paddle-wheel structure, containing a Rh–Rh bond and four bridging ligands at equatorial positions.[9–17] These catalysts have proven to be highly effective for a diverse array of asymmetric carbene transformations of diazocarbonyl compounds, including cyclopropanation, C–H activation, X–H insertion and ylide formation.[18–26] So far, various groups have focused on the immobilization of chiral dirhodium catalysts *via* equatorial[27–34] or axial[35–37] binding. In this context, Jones *et al.*[38–41] described the use of modified chiral ligands for several dirhodium catalysts, such as Rh_2(S-DOSP)$_4$, Rh_2(S-*p*-*Br*/*Ph*-TPCP)$_4$ and Rh_2(S-*o*-ClTPCP)$_4$, which were then grafted to silica particles or embedded in a hollow fiber reactor. Davies *et al.*[36,42,43] immobilized a variety of chiral dirhodium catalysts on cross-linked resins *via* axial binding. Recently, some of us designed novel chiral dirhodium coordination polymers *via* ligand exchange using $Rh_2(TFA)_4$ and chiral dicarboxylic acids as precursors.[44] These coordination polymers exhibited excellent catalytic activity in the cyclopropanation between styrene and diazooxindole. Further advantages, which set them apart from other heterogeneous catalysts, are their uniform distribution, high density, and good accessibility of their active sites. In addition, the

[a] *Technical University of Darmstadt, Institute of Inorganic and Physical Chemistry, Alarich-Weiss-Straße 8, D-64287 Darmstadt, Germany.*
E-mail: gutmann@chemie.tu-darmstadt.de, gerd.buntkowsky@chemie.tu-darmstadt.de
[b] *Free University of Berlin, Institute of Chemistry and Biochemistry, Takustraße 3, D-14195 Berlin, Germany*

† Electronic supplementary information (ESI) available. See DOI: 10.1039/d1cy00109d

employed synthetic approach is simple since it requires only a small number of preparation steps, and does not require additional solid materials. This preserves the advantages of heterogeneous catalysts such as easy catalyst separation and furthermore allows an easy recovery of rhodium as rhodium oxide after thermal combustion of the organic linker system.

However, the obtained chiral dirhodium catalysts showed only moderate enantioselectivity probably due to the chiral ligand which was synthesized from aromatic dicarboxylic acids derived from L-phenylalanine. It has been proposed in ref. 18, 45 and 46 that the enantioselectivity of homogeneous dirhodium catalysts increases with increasing steric bulk at the α-carbon of the ligands. Their study showed that the highest enantioselectivity of dirhodium catalysts is achieved in some reactions when the ligand system carries a *tert*-butyl group.

The aim of the present work is to study the effect of ligand size of chiral ligand systems carrying *tert*-butyl groups in dirhodium coordination polymers on their catalytic performance and selectivity. First, we describe the synthesis of three chiral ligands with different sizes, namely (2*S*,2′*S*)-2,2′-(4,4′-biphthalimide-*N*,*N*′-diyl)bis(3,3-dimethylbutanoic acid) (H_2L1), (2*S*,2′*S*)-2,2′-(((ethane-1,2-diylbis(oxy))bis(carbonyl))bis(1,3-dioxoisoindoline-5,2-diyl)) bis(3,3-dimethylbutanoic acid) (H_2L2), (2*S*,2′*S*)-2,2′-(((pentane-1,5-diylbis(oxy))bis(carbonyl))bis(1,3-dioxoisoindoline-5,2-diyl)) bis(3,3-dimethylbutanoic acid) (H_2L3) (structures are shown in Scheme 1). These ligand systems are then used in a ligand substitution reaction with $Rh_2(TFA)_4$ to prepare chiral dirhodium coordination polymers, abbreviated as Rh_2–L1, Rh_2–L2 and Rh_2–L3, respectively (reactions are shown in Fig. 1). The obtained chiral dirhodium coordination polymers are then characterized by various techniques including FTIR, solid-state NMR spectroscopy, DR-UV-vis and XPS. Their catalytic performances and selectivities are studied in the formation of spiro cyclopropyloxindoles from diazooxindole and aryl alkenes. Finally, their stability is tested exemplary in leaching and recycling experiments.

Experimental section

Materials

Rhodium trifluoroacetate ($Rh_2(TFA)_4$, Acros Organics), 4,4′-biphthalic dianhydride (dianhydride 1) (abcr GmbH), ethylene glycol bis(trimellitic anhydride) (dianhydride 2) (abcr GmbH), L-*tert*-leucine (abcr GmbH), trimellitic anhydride chloride (Sigma-Aldrich), 1,5-pentanediol (Acros Organics), styrene (Sigma-Aldrich), 4-fluorostyrene (abcr GmbH), 4-chlorostyrene (Acros Organics), 4-methylstyrene (Acros Organics), *N*,*N*-dimethylformamide (Sigma-Aldrich), pyridine (Carl Roth), acetic acid (Sigma-Aldrich), dichloromethane (Sigma-Aldrich), 1,2-dichloroethane (Sigma-Aldrich) and ethyl acetate (Sigma-Aldrich) were purchased and used without further purification. Phthalic anhydride of 1,5-pentanediol (dianhydride 3) was synthesized from trimellitic anhydride chloride and 1,5-pentanediol.

Synthesis of chiral diacid ligands

H_2L1. H_2L1 was synthesized according to the protocol described in ref. 47 which was partially modified. Typically, a mixture of 4,4′-biphthalic dianhydride (dianhydride 1) (2.94 g, 10 mmol) and L-*tert*-leucine (2.62 g, 20 mmol) was dissolved in acetic acid/pyridine (50 mL, 3/2 v/v) and stirred at room temperature for 2 h and then under reflux for 4 h. The solvent was removed under reduced pressure and the residue was dissolved in 50 mL of cold 2 M hydrochloric acid. The solution was stirred overnight to completely remove residual pyridine. A white precipitate was obtained. This precipitate was filtered off, washed with 200 mL of deionized water and dried under vacuum. (4.40 g, 85% yield), ^{1}H NMR (300 MHz, DMSO-d_6) δ: 12.90 (s, 2H), 8.23–8.33 (m, 4H), 8.00–8.06 (m, 2H), 4.52 (s, 2H), 1.11 (s, 18H). ^{13}C NMR (75 MHz, DMSO-d_6) δ: 169.14, 167.73, 145.20, 134.48, 132.50,

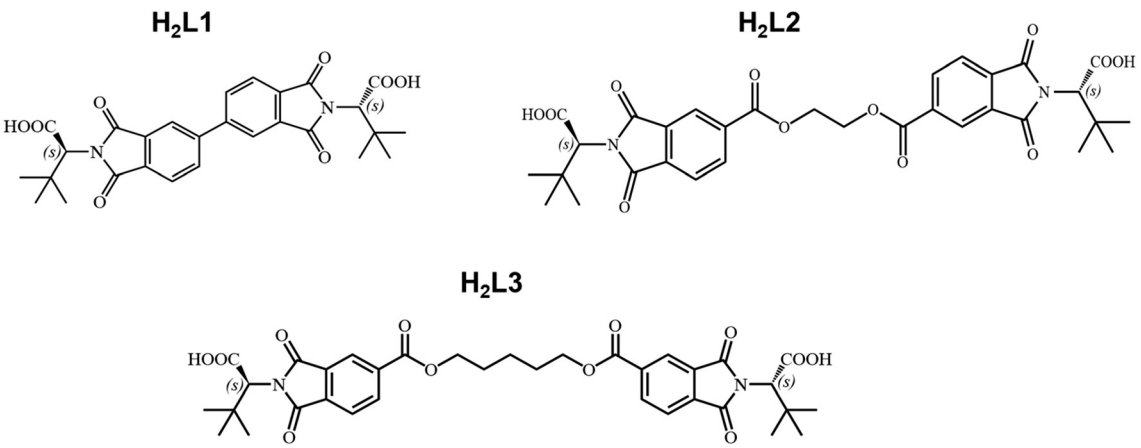

Scheme 1 Structures of the novel chiral ligand systems: (2*S*,2′*S*)-2,2′-(4,4′-biphthalimide-*N*,*N*′-diyl)bis(3,3-dimethylbutanoic acid) (H_2L1), (2*S*,2′*S*)-2,2′-(((ethane-1,2-diylbis(oxy))bis(carbonyl))bis(1,3-dioxoisoindoline-5,2-diyl)) bis(3,3-dimethylbutanoic acid) (H_2L2), (2*S*,2′*S*)-2,2′-(((pentane-1,5-diylbis(oxy))bis(carbonyl))bis(1,3-dioxoisoindoline-5,2-diyl))bis(3,3-dimethylbutanoic acid) (H_2L3).

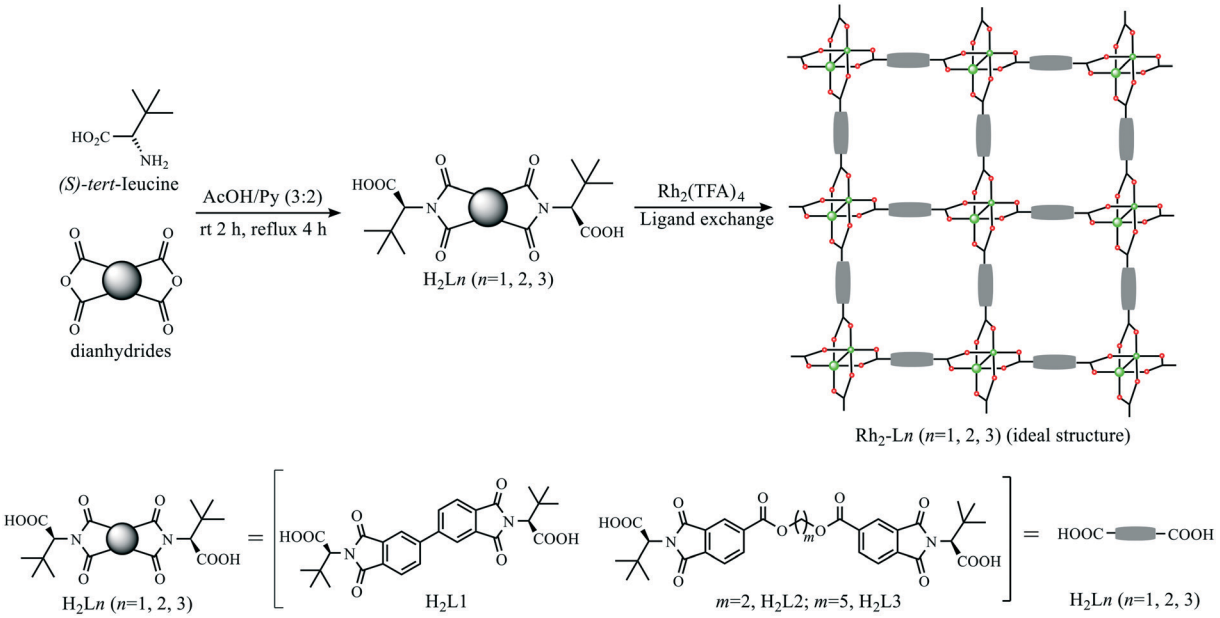

Fig. 1 Scheme for the synthesis of chiral dirhodium coordination polymers by ligand exchange. Note: Green circles refer to rhodium atoms and red circles refer to oxygen atoms.

131.22, 124.60, 123.02, 59.79, 35.47, 28.16. MS (ESI†) calcd. for $C_{28}H_{29}N_2O_8$ $[M+H]^+$: 521.1879, found 521.1918.

H_2L2. H_2L2 was synthesized similar to H_2L1. Ethylene glycol bis(trimellitic anhydride) (dianhydride 2) (2.05 g, 5 mmol) and L-*tert*-leucine (1.31 g, 10 mmol) were used as precursors. (2.77 g, 87% yield). ^{1}H NMR (300 MHz, DMSO-d_6) δ: 12.96 (s, 2H), 8.41–8.44 (dd, J = 7.7, 1.4 Hz, 2H), 8.32 (d, J = 1.3 Hz, 2H), 8.06–8.08 (d, J = 7.8 Hz, 2H), 4.76 (s, 4H), 4.51 (s, 2H), 1.10 (s, 18H). ^{13}C NMR (75 MHz, DMSO-d_6) δ: 168.46, 166.77, 164.16, 135.69, 135.15, 134.53, 131.42, 124.06, 123.51, 63.57, 59.44, 35.01, 27.60. MS (ESI†) calcd. for $C_{32}H_{33}N_2O_{12}$ $[M + H]^+$: 637.1989, found 637.2028.

Phthalic anhydride of 1,5-pentanediol (dianhydride 3). Trimellitic anhydride chloride (4.21 g, 20 mmol) and 1,5-pentanediol (1.04 g, 10 mmol) were dissolved in 30 mL dry CH_2Cl_2 and cooled to −60 °C with a dry ice/isopropanol mixture under a dry argon atmosphere. Then, under stirring 1.8 ml distilled pyridine was added dropwise to the mixture. Afterwards, it was kept at −60 °C for 2 h and then heated to room temperature for another 12 h. The obtained precipitate was collected by filtration, washed with 200 mL of deionized water, as well as 100 mL of methanol and dried under vacuum (3.43 g, yield 76%). Since the product was insoluble, no solution NMR was performed. Analysis of FT-IR data shows that the desired product was obtained. FTIR (ESI† Fig. S2): 1848/1772 cm^{-1} (acid anhydride C═O) and 1714 cm^{-1} (ester C═O) in the 1300–2000 cm^{-1} range, which is consistent with dianhydride 2. Anal. calcd. (%) for $C_{23}H_{16}O_{10}$ (452.37): C: 61.07, H: 3.57, found: C: 60.75, H: 3.64.

H_2L3. H_2L3 was synthesized similar to H_2L1 using dianhydride 3 (2.26 g, 5 mmol) and L-*tert*-leucine (1.31 g, 10 mmol) as precursors. (2.85 g, 84% yield). ^{1}H NMR (300 MHz, DMSO-d_6) δ: 12.96 (s, 2H), 8.39 (dd, J = 7.8, 1.5 Hz, 2H), 8.27 (d, J = 1.4 Hz, 2H), 8.03 (d, J = 7.8 Hz, 2H), 4.50 (s, 2H), 4.37 (t, J = 6.4 Hz, 4H), 1.83 (p, J = 6.2 Hz, 4H), 1.58 (qd, J = 8.6, 5.8 Hz, 2H), 1.09 (s, 18H). ^{13}C NMR (75 MHz, DMSO-d_6) δ: 168.47, 166.76, 164.13, 135.53, 135.48, 134.35, 131.37, 123.95, 123.33, 65.43, 59.43, 34.99, 27.60, 21.93. MS (ESI†) calcd. for $C_{35}H_{39}N_2O_{12}$ $[M + H]^+$: 679.2458, found 679.2498.

Synthesis of dirhodium coordination polymers. The novel dirhodium coordination polymers were synthesized according to our previous studies.[44,48,49] The Rh contents were calculated from the TG analysis (Fig. S1 in the ESI†) according to the method reported by Kaskel *et al.*[50]

Rh_2–L1. Rh_2–L1 was synthesized as follows. $Rh_2(TFA)_4$ (0.10 g, 0.15 mmol) and H_2L1 (0.23 g, 0.46 mmol) in 75 mL ethyl acetate (EtOAc) were charged into a 100 mL round-bottom flask, which was fitted with a Soxhlet extractor containing a mixture of 1 g K_2CO_3 and 1 g 4 Å molecular sieve in a cellulose filter tube. After 5 days of reaction under reflux, the obtained solid was filtered and washed in a Soxhlet extractor with EtOAc for another 2 days. Then, the solid was dried under vacuum yielding Rh_2–L1 (64.2 mg, 34% yield). Rh_2 content (TGA): 0.82 mmol g^{-1}, (theoretical): 0.80 mmol g^{-1}. Note: Theoretical contents were calculated for the ideal framework of dirhodium units, which are bound to two chiral ligands.

Rh_2–L2. Rh_2–L2 was synthesized similar to Rh_2–L1 using H_2L2 (0.29 g, 0.46 mmol) as a ligand. (78.2 mg, 35% yield). Rh_2 content (TGA): 0.66 mmol g^{-1}, (theoretical): 0.68 mmol g^{-1}.

Rh_2–L3. Rh_2–L3 was synthesized similar to Rh_2–L1 using H_2L3 (0.31 g, 0.46 mmol) as a ligand. (77.1 mg, 33% yield). Rh_2 content (TGA): 0.70 mmol g^{-1}, (theoretical): 0.64 mmol g^{-1}.

Catalytic asymmetric cyclopropanation

The asymmetric cyclopropanation of styrene and diazooxindole was carried out to evaluate the catalytic performance of the Rh_2–L1, Rh_2–L2 and Rh_2–L3 coordination polymer catalysts. In a typical reaction,[51,52] styrene (0.75 mmol), diazooxindole (0.15 mmol), the coordination polymer (3.75 μmol Rh_2) and dichloromethane (DCM) (3 mL) were mixed and stirred at 0 °C for 2 h under an Ar atmosphere. The catalyst was removed by filtration and the solvent was removed under reduced pressure. The yields of spiro-cyclopropyloxindoles were either determined by ^{1}H NMR analysis of the crude reaction mixture or by separation of the spiro-cyclopropyloxindoles from the crude reaction mixture by silica gel column chromatography (hexane/EtOAc = 2 : 1 to 1 : 1) (for details see the ESI†). The diastereomeric ratio (dr) was determined by ^{1}H NMR of the crude reaction mixture (for details see the ESI†). After separation of the spiro-cyclopropyloxindoles from the crude reaction mixture by silica gel column chromatography the enantiomers were separated by chiral HPLC. The enantiomeric excess (ee) was then calculated for the *trans*-enantiomers from the data determined by chiral HPLC analysis (for details see the ESI†).

Characterization

Thermogravimetric (TG) analyses were performed on a simultaneous thermal analyzer TG 209 F3 Tarsus under a purified air flow (75 mL min^{-1}). The amounts of carbon, nitrogen and hydrogen were determined on a Vario EL III Elemental Analyzer.

Fourier-transform infrared spectra (FT-IR) were measured on a Perkin Elmer Spectrum spotlight 200 FT-IR spectrometer with 4 cm^{-1} resolution.

The morphologies were examined by scanning electron microscopy (SEM), using a HITACHI S4800 instrument at 5 keV of electron beam energy.

X-ray powder diffraction (XRD) data were acquired in transmission geometry on an X-ray powder diffractometer (STADIP, Stoe & Cie GmbH, Darmstadt) using Cu-Kα_1 radiation (λ = 1.54060 Å, Ge[111]-monochromator). The samples were measured in the 2θ range of 2–60°.

^{1}H → ^{13}C CP MAS NMR spectra were recorded at room temperature on a 9.4 T Bruker Avance II+ solid state NMR spectrometer at a frequency of 100.61 MHz for ^{13}C, employing a 4 mm broadband double-resonance probe. For all samples, cross polarization experiments were measured with contact times of 1.5 ms at a spinning rate of 12 or 8.6 kHz. 3156–12 420 scans were applied with a repetition delay of 2 s. The spectra were referenced to TMS using adamantane (δ = 38.5 ppm) as an external standard.

^{19}F MAS NMR spectra were measured on a 9.4 T Bruker Avance II+ solid state NMR spectrometer at a frequency of 376.50 MHz with a 3.2 mm double-resonance probe. The spectra were recorded with single pulse excitation employing a 20° excitation pulse of 0.46 μs at a spinning rate of 15 kHz. 512 scans were applied with a long repetition delay of 300 s to ensure the acquisition of quantitative spectra. The spectra were referenced to $CFCl_3$ employing solid BaF_2 (δ = −14.35 ppm) as an external standard. BaF_2 was further used as a standard for quantification of the fluorine contents in the samples.

The diffuse reflection ultraviolet-visible spectra (DR-UV-vis) were recorded on a Jasco V-770 spectrometer equipped with a praying mantis mirror cell and a high-temperature reaction chamber (Harrick Scientific Products Inc.). Spectra were recorded from 800 to 200 nm with a spectral resolution of 0.5 nm. MgO was used as a white standard.

The surface electronic states were analyzed by X-ray photoelectron spectroscopy (XPS) using a PerkinElmer PHI 5000C ESCA system. The binding energy was calibrated by using C_{1s} = 284.8 eV as a reference.

Results and discussion

Fig. 1 depicts the synthetic route applied for the three chiral dirhodium coordination polymers. It is based on a ligand substitution approach published formerly by some of us[44,48,49] using the precursor $Rh_2(TFA)_4$ and H_2L1, H_2L2 or H_2L3 as a ligand system, respectively. In the first step, the chiral ligands were synthesized from their corresponding dianhydrides and L-*tert*-leucine. Next, these ligands were utilized to replace the TFA groups in $Rh_2(TFA)_4$ and coordinate with Rh_2 units, resulting in chiral dirhodium coordination polymers, namely Rh_2–L1, Rh_2–L2 and Rh_2–L3, respectively.

The compositions of the coordination polymers Rh_2–L*n* (*n* = 1–3) were determined by elemental analysis (C, H, N contents), TG analysis (Rh contents) and quantitative ^{19}F MAS NMR (F contents). As listed in Table 1, the experimental weight percentages of C (44.38, 51.38, 47.35 wt%), H (4.41, 4.42, 4.89 wt%) and N (3.13, 3.64, 3.05) show deviations from the theoretical contents especially for C (Rh_2–L1: 44.38 *vs.* 54.12 wt% and Rh_2–L3: 47.35 wt% *vs.* 53.92 wt%) and N (Rh_2–L1: 3.13 *vs.* 4.51 wt% and Rh_2–L3: 3.05 wt% *vs.* 3.59 wt%). The lower experimental carbon and nitrogen contents most probably refer to the presence of trifluoroacetate groups in Rh_2–L*n* (*n* = 1,3) that have not been exchanged by chiral ligands when the coordination polymers were formed. The hydrogen contents of all samples are about 0.19–0.32 wt% higher than the theoretical values. This observation may be attributed to a small amount of remaining ethyl acetate or water molecules that were not removed when drying the samples. This hypothesis is underlined by TG analyses of Rh_2–L*n* (*n* = 1–3) (ESI† Fig. S1) that show a small decrease of mass at 100 °C for each catalyst. The quantitative ^{19}F MAS NMR analysis provided a fluorine content in the Rh_2–L*n* (*n* = 1–3) coordination polymers of 5.38, 0.30 and 2.81 wt%, respectively, which indicates an incomplete ligand exchange during the synthesis of the coordination polymers especially for Rh_2–L1 and Rh_2–L3. The experimental Rh weight percentages of Rh_2–L*n* (*n* = 1–3) are 16.87, 13.54 and 14.35

Table 1 Compositions of Rh_2–L*n* (*n* = 1–3) catalysts

Sample	[a,b]Content	C (wt%)	H (wt%)	N (wt%)	Rh (wt%)	F (wt%)
Rh_2–L1	Experimental	44.38	4.41	3.13	16.87	5.38
	Theoretical	54.12	4.22	4.51	16.56	0
Rh_2–L2	Experimental	51.38	4.42	3.64	13.54	0.30
	Theoretical	52.12	4.10	3.80	13.95	0
Rh_2–L3	Experimental	47.35	4.89	3.05	14.35	2.81
	Theoretical	53.92	4.65	3.59	13.20	0

[a] Experimental contents were determined by elemental analysis (C, H, N), TG analysis (Rh), and quantitative ^{19}F MAS NMR (F). [b] Theoretical contents were calculated for the ideal framework of dirhodium units, which are bound to two chiral H_2L*n* (*n* = 1–3) groups.

wt%, which are almost equal to the predicted theoretical values 16.56, 13.95 and 13.20 wt%, respectively.

The morphologies and crystallinity of the polymers were explored by SEM and XRD, respectively. Fig. 2a–c show the SEM images of Rh_2–L1, Rh_2–L2 and Rh_2–L3, respectively. All samples display 2D disordered lamellar structures that are arranged as plates/flakes. The XRD patterns (Fig. 2d) of the three polymers exhibit broad background modulations suggesting a random stacking of the dirhodium coordination polymers.

The FT-IR spectra in the range between 1900 and 1300 cm^{-1} of Rh_2–L*n* (*n* = 1–3) and their parent diacids are shown in Fig. 3. The adsorption bands around 1775 and 1715 cm^{-1} are characteristic for the C═O asymmetric and symmetric vibration of the imide moiety,[50,53,54] which are present in all ligand systems and coordination polymers. The bands at around 1482 and 1378 cm^{-1} are assigned to C═C vibrations of aromatic rings and C–N stretching vibrations, respectively.

In the spectra of H_2L*n* (*n* = 1–3), the C═O of the carboxyl moieties is visible as signals at 1612 cm^{-1} (symmetric stretching vibration) and 1637 cm^{-1} (asymmetric stretching vibration). The band at 1612 cm^{-1} has almost disappeared and a new one at around 1595 cm^{-1} has appeared in the Rh_2–L*n* (*n* = 1–3) spectra. This tiny shift of the C═O symmetric stretching vibration is most probably related to COOH groups of H_2L*n* that coordinate with the dirhodium units. Note that the small vibration around 1595 cm^{-1} in the $Rh_2(TFA)_4$ spectrum (Fig. 3a) may be attributed to small amounts of acetate groups present in the $Rh_2(TFA)_4$ precursor as has been discussed in previous studies.[44,48,49]

In addition, vibrations of C═O of the trifluoroacetate group at 1637 and 1463 cm^{-1} are visible in the spectrum of the precursor $Rh_2(TFA)_4$ (Fig. 3a), while the adsorption at 1463 cm^{-1} is not observed in the obtained Rh_2–L*n* coordination polymers. This indicates that TFA groups of $Rh_2(TFA)_4$ were replaced by chiral ligands during the

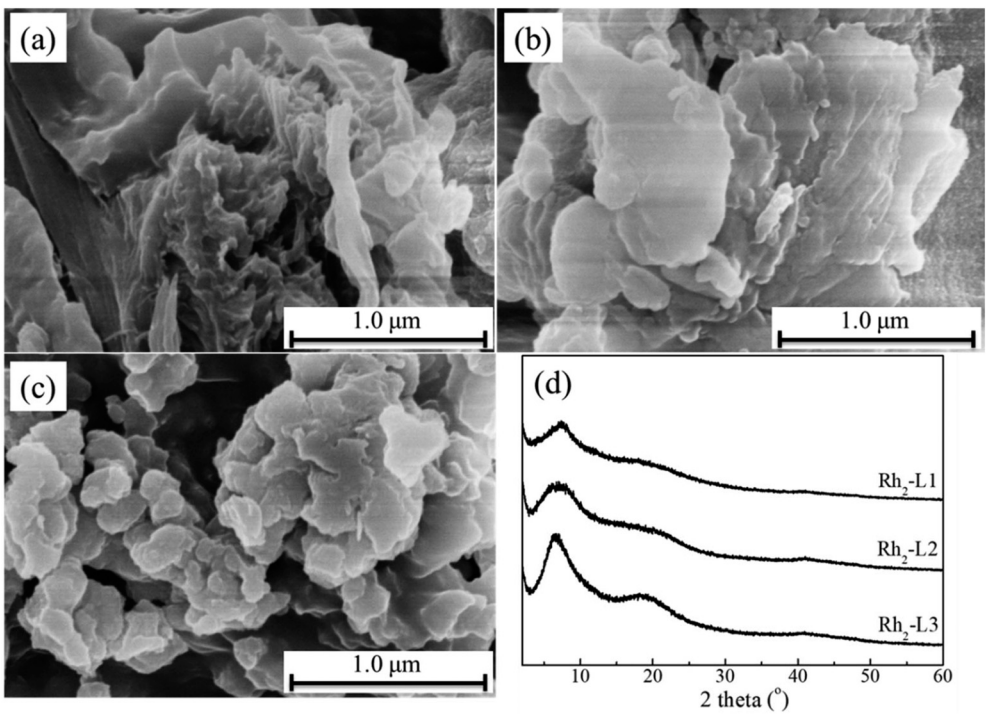

Fig. 2 SEM images of (a) Rh_2–L1, (b) Rh_2–L2, and (c) Rh_2–L3. (d) XRD patterns of Rh_2–L*n* (*n* = 1–3) samples.

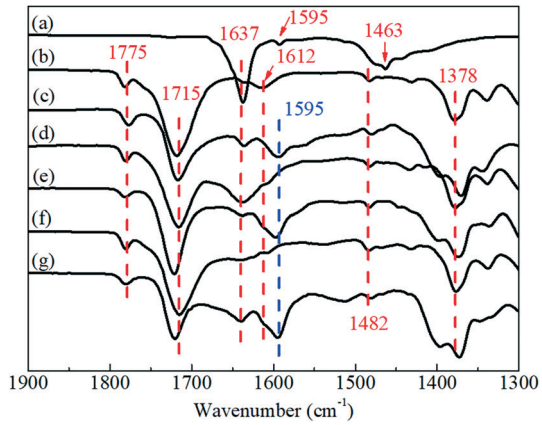

Fig. 3 FT-IR spectra in the range between 1900 and 1300 cm^{-1} of (a) $Rh_2(TFA)_4$, (b) H_2L1, (c) Rh_2–L1, (d) H_2L2 and (e) Rh_2–L2, (f) H_2L3 and (g) Rh_2–L3. Spectra were normalized on the intensity of the signals at 1775 and 1715 cm^{-1}.

synthesis of the coordination polymers.[44] These observations from the FT-IR spectra strongly indicate the success of ligand exchange between $Rh_2(TFA)_4$ and H_2Ln.

Fig. 4b–g show the $^1H \rightarrow {}^{13}C$ CP MAS NMR spectra of H_2Ln and Rh_2–Ln (n = 1–3). The visible signals around 26 and 35 ppm are characteristic for the carbon atoms of the –C–$(\underline{C}H_3)_3$ and –$\underline{C}$–$(CH_3)_3$ groups, respectively. The small peak around 61 ppm is assigned to carbon atoms of the –N–$\underline{C}$HR–$C(CH_3)_3$ (R=–COOH) groups. The peak at 66 ppm which is only observed in the spectra of H_2L2, Rh_2–L2, H_2L3 and Rh_2–L3, respectively, most probably refers to –O–$\underline{C}H_2$– groups. The overlapping peaks in the range between 120 and 145 ppm correspond to aromatic carbons and the broad signals in the range between 160 and 180 ppm are assigned to C═O groups in different chemical environments. Deconvolution of these signals allows us to identify C═O groups in imide (around 167 ppm), C═O groups in esters (around 164 ppm) and C═O groups in carboxylic groups (around 171 ppm). The chemical shifts of appropriate signals slightly differ for these groups, which is probably caused by functional groups that generate different local environments on the carbonyl carbons. The signal at 171 ppm is slightly up-field shifted compared to the signal of C═O groups in carboxylic groups obtained in our previous work (around 177 ppm).[44] This observation is most probably related to the substituent at the α-carbon which in the present work is the *tert*-butyl group while in the former work it was benzyl.

More importantly, in the spectra of the coordination polymers a new broad signal from 180 to 195 ppm appears

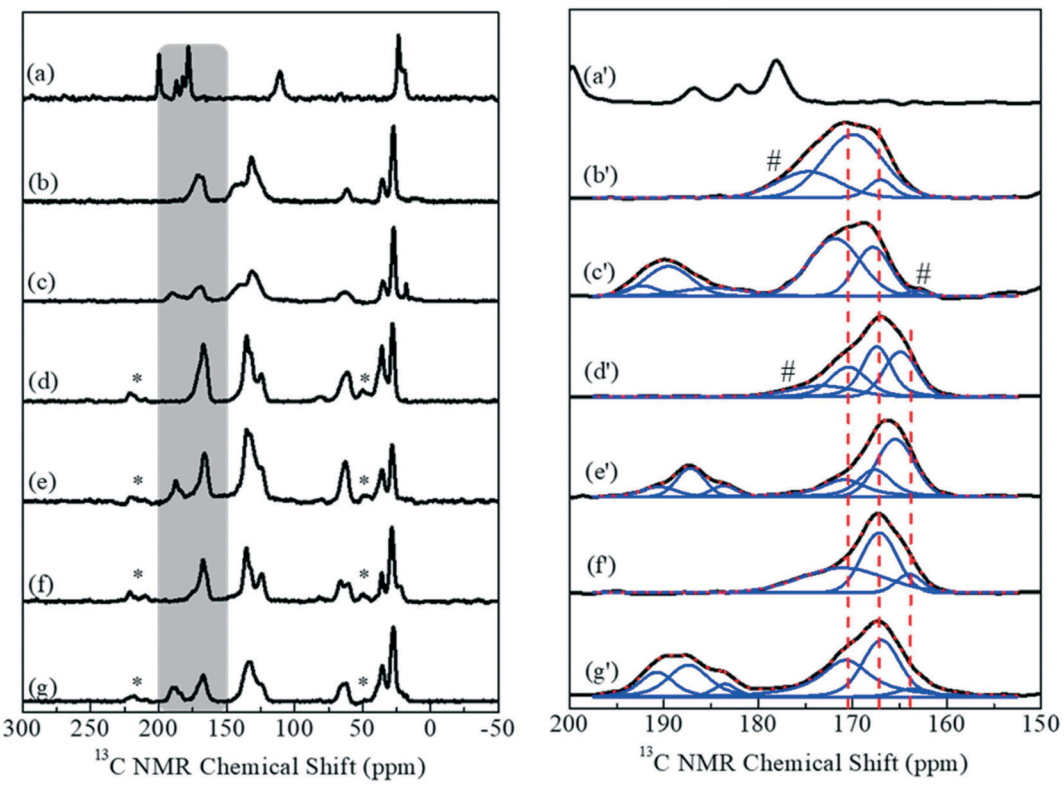

Fig. 4 $^1H \rightarrow {}^{13}C$ CP MAS NMR spectra (left panel) zoomed in the spectral range between 150 and 200 ppm showing the deconvolution performed with Voigt functions (right panel) of $Rh_2(TFA)_4$ (a and a′), H_2L1 (b and b′), Rh_2–L1 (c and c′), H_2L2 (d and d′), Rh_2–L2 (e and e′), H_2L3 (f and f′) and Rh_2–L3 (g and g′). Note: The spectra of $Rh_2(TFA)_4$, H_2L1 and Rh_2–L1 were recorded at 9.4 Tesla with 12 kHz spinning, the spectra of H_2L2, Rh_2–L2, H_2L3 and Rh_2–L3 were recorded at 9.4 Tesla with 8.6 kHz spinning. Signals marked with * are spinning side bands of the phenyl group (134 ppm) with an ester chain. The signals marked with # cannot be assigned to specific functional groups. They were included in the deconvolution to represent the spectral shape in a better way. The dashed lines are shown to guide the eyes.

which consists of several single signals. The dominant signal around 188 ppm stems most probably from C═O groups in COO^-, which coordinate with Rh_2 units. The additional signals around 184 and 191 ppm may be due to adsorbed acetic acid or coordinated acetate.[14,48,49] Surprisingly, the signal at 171 ppm has not disappeared in the spectrum of Rh_2–L*n*, which indicates that free COOH groups are preserved in the synthesis of the coordination polymers, probably due to incomplete ligand exchange or single site coordination of the ligand systems to the dirhodium.

To investigate the quantity of the formation process, a detailed analysis of the ^{19}F MAS NMR spectra was performed. As shown in Fig. 5(I) and ESI† section 3, in all ^{19}F MAS spectra a signal centred at −74.4 is observed. This clearly demonstrates the presence of trifluoroacetate groups in all three dirhodium coordination polymers.[44] Quantitative analysis of this signal was performed to determine the amount of ^{19}F and thus the amount of TFA groups in Rh_2–L1, Rh_2–L2 and Rh_2–L3 (see ESI† section 3). From this analysis, 0.94, 0.05 and 0.49 mmol g^{-1} of TFA were determined for the three catalysts, respectively. Thus, 71%, 98% and 82% of the TFA groups are assumed to be substituted during the synthesis of Rh_2–L1, Rh_2–L2 and Rh_2–L3, respectively.

These results show that the TFA groups of $Rh_2(TFA)_4$ are almost completely replaced in Rh_2–L2. In contrast, a significant amount of TFA groups (~29%) is preserved in Rh_2–L1. This implies that TFA groups are not easily replaced by H_2L1. The replacement of TFA groups and connection of two dirhodium units by a ligand with short size seems to be limited due to the large steric hindrance. Otherwise, when the ligand size increases, the carboxyl groups of a bifunctional ligand system may easily coordinate in a single coordination mode with the same dirhodium unit at different sites, as is the case for $Rh_2(esp)_2$ (ref. 55) and Rh_2(R-KC4N)$_2$ (ref. 10) or in a double coordination mode that may connect different dirhodium units. Both possibilities are illustrated in (Fig. 5(II)). From the geometry of single coordination sites, it can be assumed that a larger amount of TFA groups is preserved. This most probably explains why Rh_2–L3 contains a larger amount of TFA groups compared to Rh_2–L2.

The dirhodium units as the catalytic site are vital for the catalytic properties, therefore the chemical environments of rhodium in the obtained polymers were investigated by DR-UV-vis and XPS. The DR-UV-vis spectra of $Rh_2(TFA)_4$, Rh_2–L1, Rh_2–L2 and Rh_2–L3 are shown in Fig. 6. Two bands are clearly visible in all spectra. The one (named as band II) which has its maximum at *ca.* 452 nm in the spectrum of $Rh_2(TFA)_4$ (Fig. 6a) is visible as a broad shoulder in the spectra of Rh_2–L1, Rh_2–L2 and Rh_2–L3 (Fig. 6b–d). The assignment of band II is uncertain, although it has been attributed to π*(Rh–Rh) → σ*(Rh–O) transitions in the literature.[56,57] Next to band II, a second one (named as band I) is clearly visible at longer wavelengths and is assigned to the HOMO–LUMO π* (Rh_2) → σ*(Rh_2) transition. Compared to the maximum of band I for $Rh_2(TFA)_4$ (Fig. 6a) which is located at 596 nm, this maximum is shifted to longer wavelengths for Rh_2–L1, Rh_2–L2 and Rh_2–L3 (Fig. 6b–d). This observation clearly suggests that TFA groups of $Rh_2(TFA)_4$ having an electron withdrawing effect are exchanged by the chiral ligand systems that typically have a less electron withdrawing effect. This leads to a change of the electronic environment at Rh_2 which reduces the energy gap between the HOMO and LUMO and thus yield a red shift of band I in the spectra of Rh_2–L1, Rh_2–L2 and Rh_2–L3 compared to $Rh_2(TFA)_4$. Detailed analysis shows that Rh_2–L1 exhibits a different position of band I (605 nm) in contrast to Rh_2–L2 and Rh_2–L3 (624 nm). A possible explanation for this observation is the structure of the ligand system. While the

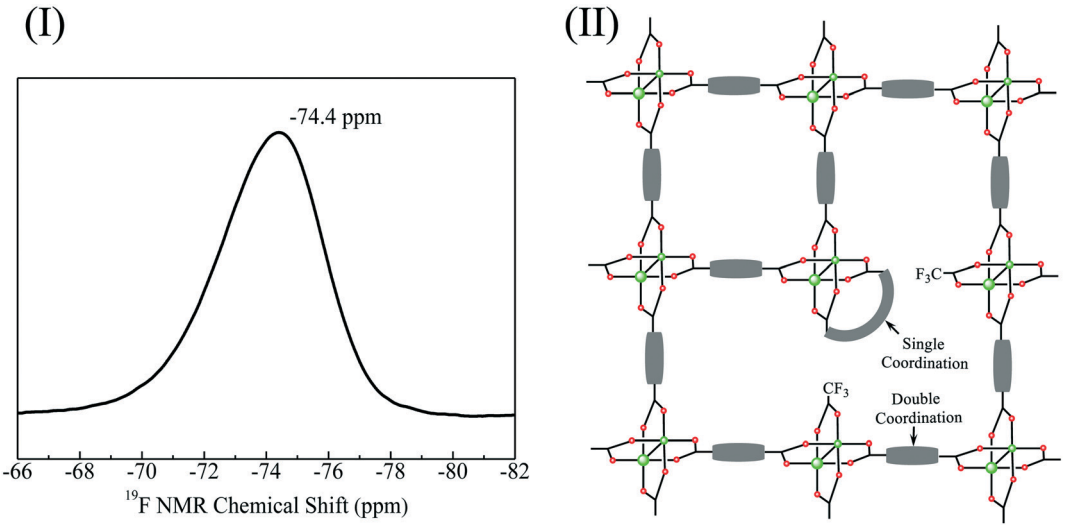

Fig. 5 (I) Zoomed in ^{19}F MAS NMR spectrum of Rh_2–L1 showing a single isotropic signal at 74.4 ppm. Note: The ^{19}F MAS spectra of Rh_2–L2 and Rh_2–L3 show the same single signal but with different intensity. Spectra and their detailed quantitative analysis are given in ESI† section 3. (II) Scheme of possible coordination of large size ligand systems illustrating that in the vicinity of single coordination sites the probability to find CF_3 groups in the close environment is high.

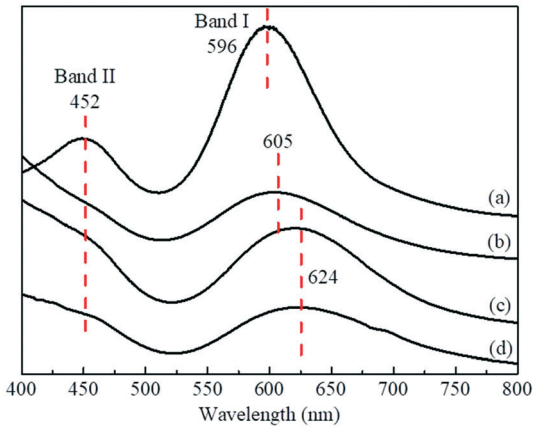

Fig. 6 DR-UV-vis spectra of (a) $Rh_2(TFA)_4$, (b) Rh_2–L1, (c) Rh_2–L2 and (d) Rh_2–L3.

structures of H_2L2 and H_3L3 are very similar (both contain a 1,3-dioxo-2,3-dihydro-isoindole-5-carboxyl moiety) they strongly differ from the structure of H_2L1 (contains a 4,4′-biphthalimide moiety) which may account for the different positions of band I. Secondly, band I is highly sensitive to additional axial interaction as shown in the literature.[56,57] The interaction between Rh_2 units and oxygen atoms of the ester group in Rh_2–L2 and Rh_2–L3 may influence the position of band I in the spectra of the dirhodium coordination polymers which has also been discussed in a former study by some of us.[44,48,49] Finally, the different amounts of preserved TFA groups in H_2L1, H_2L2 and H_3L3 after exchange and their distribution may have an influence on the position of band I. To address this more in detail quantum chemical calculations on model systems are required which are however beyond the scope of the present work.

The XPS spectra of Rh_2–L1, Rh_2–L2 and Rh_2–L3 (Fig. 7) show major peaks with binding energies around 308.9 and 313.7 eV that are assigned to Rh $3d_{5/2}$ and $3d_{3/2}$,[44,56] respectively. In contrast, the parent $Rh_2(TFA)_4$ shows significantly different binding energies of 309.4 and 314.9 eV.[44] This change in binding energies between the

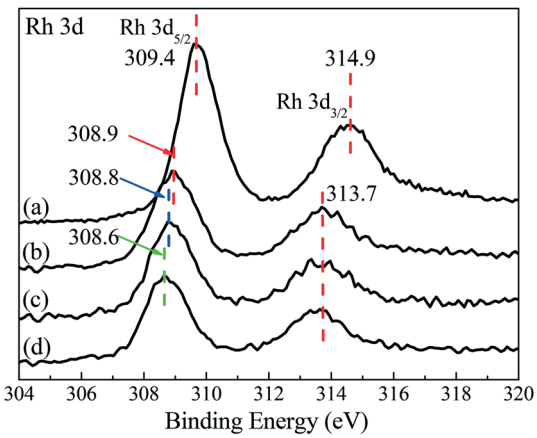

Fig. 7 XPS spectra of (a) $Rh_2(TFA)_4$, (b) Rh_2–L1, (c) Rh_2–L2 and (d) Rh_2–L3.

coordination polymers and the parent $Rh_2(TFA)_4$ underlines the success of the ligand exchange. Furthermore, for the Rh $3d_{5/2}$ signal the tendency is observed that with increasing ligand size the binding energy becomes smaller (308.9 eV for Rh_2–L1, 308.8 eV for Rh_2–L2 and 308.6 eV for Rh_2–L3). This result indicates that the electronic environment of the Rh species is different in the three dirhodium polymers,[58] which probably influences the catalytic performance in the asymmetric cyclopropanation of diazooxindole and styrene.

To validate the catalytic performance of the Rh_2–L1, Rh_2–L2 and Rh_2–L3 coordination polymers, the preparation of spiro-cyclopropyloxindoles from diazooxindole and styrene by asymmetric cyclopropanation in DCM was employed as the model reaction. Typically, in this model reaction the four isomers (*cis*-cyclopropyloxindole: *R*,*R*- and *S*,*S*-spiro-cyclopropyloxindole; *trans*-cyclopropyloxindole: *R*,*S*- and *S*,*R*-spiro-cyclopropyloxindole) are formed (see Scheme 2). As illustrated in Fig. 8a, the overall yields of spiro-cyclopropyloxindoles increase with the reaction time and are determined as 79.1% for Rh_2–L1, 90.4% for Rh_2–L2 and 94.8% for Rh_2–L3, respectively, after 120 min of reaction. Next, the diastereomeric ratios (ratio between *trans* and *cis* isomers) of spiro-cyclopropyloxindole were analyzed by ^{1}H NMR for the three catalysts. During the reaction, mole fractions of 81%, 86% and 91% of the *trans*-isomers are obtained (Fig. 8b) for the three catalysts, respectively. This ratio remains unchanged during the whole reaction time.

Finally, the enantioselectivity with respect to one of the two *trans*-enantiomers was determined *via* separation of the enantiomers by chiral HPLC. For the *cis*-enantiomers this analysis was not done due to their low amount. Employing DCM as a solvent the tendency is observed that Rh_2–L3 gives a higher ee value for one of the *trans*-enantiomers (42.9%) compared to 11.2% for Rh_2–L1 and 30.5% for Rh_2–L2 as shown in Table 2, entries 1–3.

For comparison, previously synthesized dirhodium polymers from aromatic dicarboxylic acids with L-phenylalanine only showed 13% ee for one of the *trans*-enantiomers in this reaction.[44] This clearly demonstrates that the enantioselectivity of the novel dirhodium coordination polymers is significantly improved by introducing *tert*-butyl groups into the ligand system. Compared with the homogeneous Rh_2(S-PTTL)$_4$ employed by Arai *et al.*[51] (66% ee), the heterogeneous Rh_2–L3 coordination polymer (42.9%) comes close to this value.

Based on the results from catalytic experiments on Rh_2–L*n* (*n* = 1–3), we assume that the size of the ligand system significantly influences the catalytic performance of the dirhodium coordination polymer. Rh_2–L1 contains ligands with the shortest length. This is reflected in the lowest yield and selectivity. Rh_2–L3 contains ligands with the longest length. Thus, Rh_2–L3 shows the highest yield and selectivity. Interestingly, Rh_2–L1 and Rh_2–L3 contain the largest number of non-exchanged TFA groups (see section on quantitative ^{19}F NMR). This indicates that the amount of remaining TFA sites is not the main factor that affects the selectivity of the

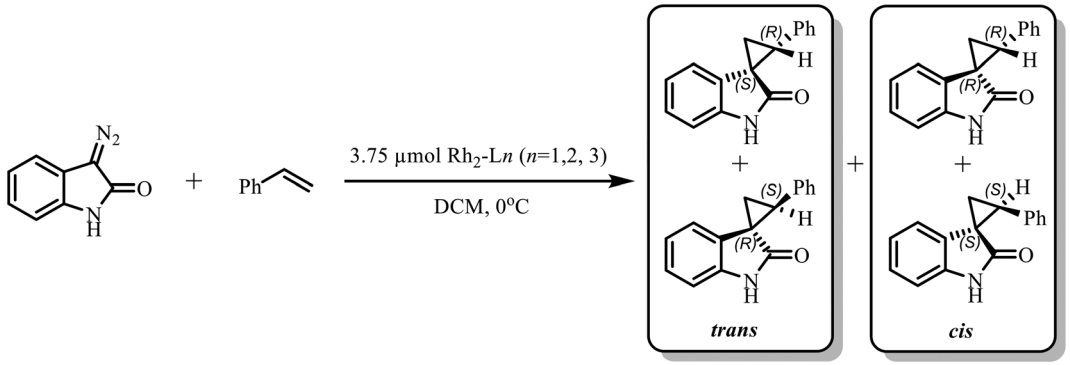

Scheme 2 Asymmetric cyclopropanation reaction of diazooxindole and styrene forming four spiro-cyclopropyloxindole isomers.

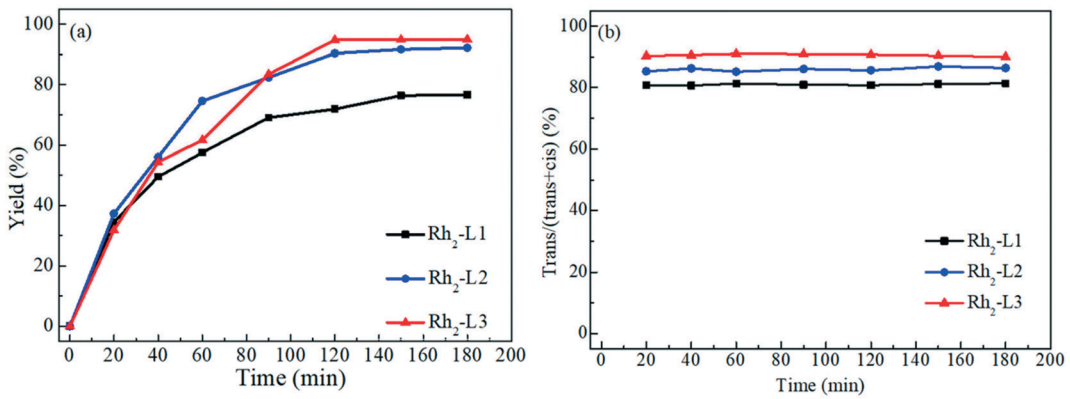

Fig. 8 Catalytic performance of the Rh_2–L*n* catalysts: (a) overall yields of spiro-cyclopropyloxindoles and (b) percentages of *trans*/(*trans* + *cis*) as functions of the reaction time were determined from ^{1}H NMR of the crude reaction mixture. Note: The lines are used to guide the eyes.

coordination polymers. The microenvironment of the Rh_2 units is most probably responsible for the obtained enantioselectivity of the coordination polymers. The XPS data shown in Fig. 7 suggest that the Rh_2–L*n* (n = 1–3) coordination polymers have slightly different Rh $3d_{5/2}$ electron binding energy. This is an indication that the catalytically active Rh_2 sites in Rh_2–L*n* (n = 1–3) contain different chiral microenvironments.

In the next step, the influence of common solvents, *i.e.* dichloromethane (DCM) and 1,2-dichoroethane (DCE), on this model reaction was inspected for the Rh_2–L3 catalyst. The analysis (Table 2, entries 3–4) shows that Rh_2–L3 produces a similar yield and diastereomeric ratio in DCM and DCE. However, the enantioselectivity is lower in DCE compared to DCM. Thus, the following experiments were all performed in DCM.

To demonstrate the universal applicability of coordination polymer Rh_2–L3, a variety of aryl alkenes were examined to prepare spiro-cyclopropyloxindoles (Scheme 3), which are an important group of heterocycles with potential application in medical research, including their use as potent HIV inhibitors[59,60] and antitumor agents.[61,62] As shown in Table 2, under the same conditions, various derivatives of styrene with electron-withdrawing or electron-donating groups at the *para*-position can be utilized for this reaction. 4-Fluorostyrene reacts with 3-diazooxindole and gives the product in 92.9% yield with 91 : 9 dr and 41.2% ee (Table 2, entry 5). 4-Methylstyrene, 4-chlorostyrene and 4-bromostyrene lead to the corresponding products with similar yield compared to 4-fluorostyrene (Table 2 entries 6–8). The enantioselectivity with respect to one of the *trans*-enantiomers in the product mixture is 51.1%, 51.8%, and 50.1%, respectively. These results confirm that Rh_2–L3 is a potent catalyst with large applicability in the asymmetric cyclopropanation to prepare spiro-cyclopropyloxindoles.

Finally, the recyclability and leaching properties of the novel coordination polymers were investigated. Since Rh_2–L3 shows the highest catalytic performance compared with Rh_2–L1 and Rh_2–L2 during the asymmetric cyclopropanation reaction between diazooxindole and styrene, this catalyst was chosen as the model system. As shown in Table 3, no significant decrease in yields, diastereomeric ratios and enantioselectivities was found after Rh_2–L3 was used repetitively five times. Furthermore, the FT-IR spectra in the range between 1900 and 1300 cm^{-1} of (a) freshly prepared Rh_2–L3, and (b) after five reaction cycles of Rh_2–L3 are compared in Fig. S3.† Both spectra show no differences in their signal patterns, which clearly indicates that the structure of Rh_2–L3 is preserved in the catalytic reaction. This demonstrates that this dirhodium coordination polymer has

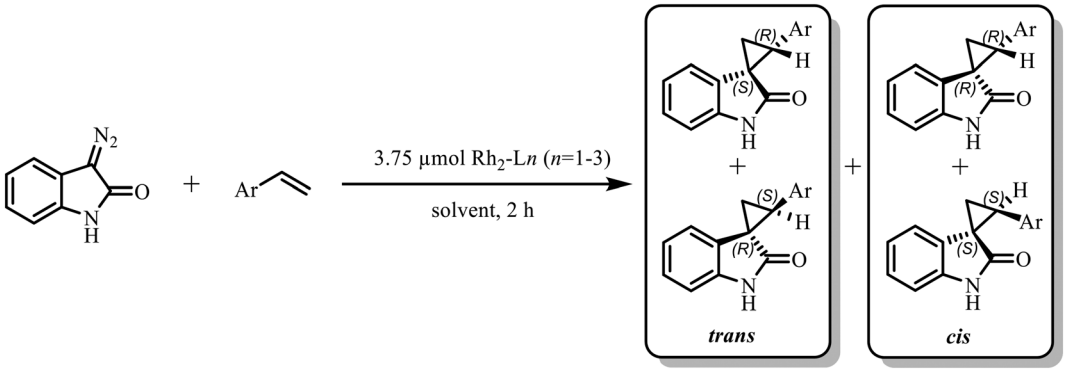

Scheme 3 Asymmetric cyclopropanation reaction of diazooxindole with different aryl alkenes (Ar=Ph, 4-FC_6H_4, 4-MeC_6H_4, 4-BrC_6H_4 or 4-ClC_6H_4, see Table 2).

Table 2 Yields, diastereomeric ratios (dr) and enantiomeric excess for one of the trans isomers (ee of *trans*) obtained in the asymmetric cyclopropanation reaction of diazooxindole with different aryl alkenes employing the coordination polymer catalysts Rh_2–L1, Rh_2–L2 and Rh_2–L3, respectively. Reaction conditions: alkenes (0.75 mmol) and diazooxindole (0.15 mmol) in solvent (3 mL) were added to a two-neck round-bottom flask containing a magnetic stir bar under an Ar atmosphere at 0 °C, then 3.75 μmol of the chiral dirhodium catalyst was added and then stirred for 2 h

Entry	Catalysts	Ar	Solvents	[a]Yield (%)	[b]dr (*trans*:*cis*)	[c]ee of *trans* (%)
1	Rh_2–L1	Ph	DCM	71.9	81:19	11.2
2	Rh_2–L2	Ph	DCM	90.4	86:14	30.5
3	Rh_2–L3	Ph	DCM	94.8	91:9	42.9
4	Rh_2–L3	Ph	DCE	95.2	90:10	35.8
5	Rh_2–L3	4-FC_6H_4	DCM	92.9	91:9	41.2
6	Rh_2–L3	4-MeC_6H_4	DCM	93.1	89:11	51.1
7	Rh_2–L3	4-ClC_6H_4	DCM	89.5	90:10	51.8
8	Rh_2–L3	4-BrC_6H_4	DCM	91.4	89:11	50.1

[a] Combined yield of diastereomers obtained by purification of the product *via* silica gel chromatography. [b] Determined by ^1H NMR analysis of the crude reaction mixture. [c] Determined by analysis of chiral HPLC data.

Table 3 Recyclability tests of Rh_2–L3 in the asymmetric cyclopropanation reaction between styrene and diazooxindole

[a]Cycle	1	2	3	4	5
[b]Yield (%)	94.8	93.2	94.1	92.4	90.1
[c]dr (*trans*:*cis*)	91:9	90:10	92:8	90:10	91:9
[d]ee (%)	42.9	40.9	41.4	40.3	39.9

[a] The catalyst was collected by filtration, washed and recycled. [b] Combined yield of diastereomers obtained by purification of the product *via* silica gel chromatography. [c] Determined from ^1H NMR of the crude reaction mixture. [d] Determined by analysis of chiral HPLC data.

excellent stability and reusability. ICP-OES analysis shows that Rh leaching is negligible in the liquid phase after the first cycle (ESI† Table S3). The leaching level is consistent with our previous work and confirms that rhodium is not prone to leaching from the dirhodium coordination polymers.

Conclusion

In summary, we further developed a ligand exchange approach to prepare chiral dirhodium coordination polymers from the precursor $Rh_2(TFA)_4$ and chiral dicarboxylic acids. These obtained polymers were characterized by various techniques including FTIR, XPS and $^1H \rightarrow {}^{13}C$ CP MAS NMR spectroscopy, revealing the successful ligand exchange. The degree of the ligand exchange was monitored by ^{19}F MAS NMR showing differences in the efficiency of ligand exchange which strongly depends on the ligand size. The SEM images and XRD data suggest that the polymers have a lamellar structure, which is randomly stacked. DR-UV-vis and XPS data demonstrated that the dirhodium unit remained intact during the synthesis of the coordination polymers. Rh_2–L3 exhibited higher catalytic activity and enantioselectivity in the asymmetric cyclopropanation reaction between diazooxindole and styrene compared with Rh_2–L1 and Rh_2–L2. This correlates with the size of the ligand systems. More importantly, the enantioselectivity has been significantly improved compared with previous dirhodium polymers. Finally, Rh_2–L3 could be easily recycled by filtration and reused five times in a test run without significant loss of catalytic activity and enantioselectivity.

Conflicts of interest

There are no conflicts to declare.

Acknowledgements

Financial support by the Deutsche Forschungsgemeinschaft under contract Bu-911-27-1 is gratefully acknowledged.

References

1 R. H. Crabtree, *The organometallic chemistry of the transition metals*, John Wiley & Sons, 2009.
2 D. E. De Vos, M. Dams, B. F. Sels and P. A. Jacobs, *Chem. Rev.*, 2002, **102**, 3615–3640.
3 A. Corma and H. Garcia, *Adv. Synth. Catal.*, 2006, **348**, 1391–1412.
4 J. Liu, P. B. Groszewicz, Q. Wen, A. S. L. Thankamony, B. Zhang, U. Kunz, G. Sauer, Y. Xu, T. Gutmann and G. Buntkowsky, *J. Phys. Chem. C*, 2017, **121**, 17409–17416.
5 X. Zhao, X. Y. Bao, W. Guo and F. Y. Lee, *Mater. Today*, 2006, **9**, 32–39.
6 M. Lamblin, L. Nassar-Hardy, J. C. Hierso, E. Fouquet and F. X. Felpin, *Adv. Synth. Catal.*, 2010, **352**, 33–79.
7 C. Coperet, M. Chabanas, R. Petroff Saint-Arroman and J. M. Basset, *Angew. Chem., Int. Ed.*, 2003, **42**, 156–181.
8 Y. Wei, Z. Mao, Z. Li, F. Zhang and H. Li, *ACS Appl. Mater. Interfaces*, 2018, **10**, 13914–13923.
9 D. T. Boruta, O. Dmitrenko, G. P. Yap and J. M. Fox, *Chem. Sci.*, 2012, **3**, 1589–1593.
10 P.-A. Chen, K. Setthakarn and J. A. May, *ACS Catal.*, 2017, **7**, 6155–6161.
11 A. DeAngelis, O. Dmitrenko, G. P. Yap and J. M. Fox, *J. Am. Chem. Soc.*, 2009, **131**, 7230–7231.
12 M. El-Deftar, G. Adly, M. G. Gardiner and A. Ghanem, *Curr. Org. Chem.*, 2012, **16**, 1808–1836.
13 S. K. Gadakh, S. Dey and A. Sudalai, *J. Org. Chem.*, 2015, **80**, 11544–11550.
14 T. Gutmann, J. Liu, N. Rothermel, Y. Xu, E. Jaumann, M. Werner, H. Breitzke, S. T. Sigurdsson and G. Buntkowsky, *Chem. – Eur. J.*, 2015, **21**, 3798–3805.
15 Z. Li and H. M. Davies, *J. Am. Chem. Soc.*, 2010, **132**, 396–401.
16 J. Liu, A. Plog, P. Groszewicz, L. Zhao, Y. Xu, H. Breitzke, A. Stark, R. Hoffmann, T. Gutmann and K. Zhang, *Chem. – Eur. J.*, 2015, **21**, 12414–12420.
17 D. Rackl, C.-J. Yoo, C. W. Jones and H. M. Davies, *Org. Lett.*, 2017, **19**, 3055–3058.
18 F. G. Adly, M. G. Gardiner and A. Ghanem, *Chem. – Eur. J.*, 2016, **22**, 3447–3461.
19 H. M. Davies and J. R. Denton, *Chem. Soc. Rev.*, 2009, **38**, 3061–3071.
20 H. M. Davies and J. R. Manning, *Nature*, 2008, **451**, 417–424.
21 H. M. Davies and D. Morton, *Chem. Soc. Rev.*, 2011, **40**, 1857–1869.
22 M. P. Doyle, R. Duffy, M. Ratnikov and L. Zhou, *Chem. Rev.*, 2010, **110**, 704–724.
23 P. M. Gois and C. A. Afonso, *Eur. J. Org. Chem.*, 2004, **2004**, 3773–3788.
24 M.-Y. Huang, J.-M. Yang, Y.-T. Zhao and S.-F. Zhu, *ACS Catal.*, 2019, **9**, 5353–5357.
25 T. Miyazawa, K. Minami, M. Ito, M. Anada, S. Matsunaga and S. Hashimoto, *Tetrahedron*, 2016, **72**, 3939–3947.
26 R. P. Reddy, G. H. Lee and H. M. Davies, *Org. Lett.*, 2006, **8**, 3437–3440.
27 L. Chen, T. Yang, H. Cui, T. Cai, L. Zhang and C.-Y. Su, *J. Mater. Chem. A*, 2015, **3**, 20201–20209.
28 M. P. Doyle, D. J. Timmons, J. S. Tumonis, H.-M. Gau and E. C. Blossey, *Organometallics*, 2002, **21**, 1747–1749.
29 M. P. Doyle, M. Yan, H.-M. Gau and E. C. Blossey, *Org. Lett.*, 2003, **5**, 561–563.
30 H. M. Hultman, M. de Lang, M. Nowotny, I. W. Arends, U. Hanefeld, R. A. Sheldon and T. Maschmeyer, *J. Catal.*, 2003, **217**, 264–274.
31 T. Oohara, H. Nambu, M. Anada, K. Takeda and S. Hashimoto, *Adv. Synth. Catal.*, 2012, **354**, 2331–2338.
32 K. Takeda, T. Oohara, M. Anada, H. Nambu and S. Hashimoto, *Angew. Chem., Int. Ed.*, 2010, **49**, 6979–6983.
33 K. Takeda, T. Oohara, N. Shimada, H. Nambu and S. Hashimoto, *Chem. – Eur. J.*, 2011, **17**, 13992–13998.
34 B. Zhu, G. Liu, L. Chen, L. Qiu, L. Chen, J. Zhang, L. Zhang, M. Barboiu, R. Si and C.-Y. Su, *Inorg. Chem. Front.*, 2016, **3**, 702–710.
35 F. G. Adly and A. Ghanem, *Tetrahedron Lett.*, 2016, **57**, 852–857.
36 H. M. Davies, A. M. Walji and T. Nagashima, *J. Am. Chem. Soc.*, 2004, **126**, 4271–4280.
37 A. F. Trindade, J. A. Coelho, C. A. Afonso, L. F. Veiros and P. M. Gois, *ACS Catal.*, 2012, **2**, 370–383.
38 T. A. Hatridge, W. Liu, C.-J. Yoo, H. M. Davies and C. W. Jones, *Angew. Chem., Int. Ed.*, 2020, **59**, 19525–19531.
39 E. G. Moschetta, S. Negretti, K. M. Chepiga, N. A. Brunelli, Y. Labreche, Y. Feng, F. Rezaei, R. P. Lively, W. J. Koros and H. M. Davies, *Angew. Chem., Int. Ed.*, 2015, **54**, 6470–6474.
40 C. J. Yoo, D. Rackl, W. Liu, C. B. Hoyt, B. Pimentel, R. P. Lively, H. M. Davies and C. W. Jones, *Angew. Chem., Int. Ed.*, 2018, **57**, 10923–10927.
41 K. M. Chepiga, Y. Feng, N. A. Brunelli, C. W. Jones and H. M. Davies, *Org. Lett.*, 2013, **15**, 6136–6139.
42 H. M. Davies and A. M. Walji, *Org. Lett.*, 2003, **5**, 479–482.
43 H. M. Davies and A. M. Walji, *Org. Lett.*, 2005, **7**, 2941–2944.
44 Z. Li, L. Rösler, K. Herr, M. Brodrecht, H. Breitzke, K. Hofmann, H.-H. Limbach, T. Gutmann and G. Buntkowsky, *ChemPlusChem*, 2020, **85**, 1737–1746.
45 K. Minami, H. Saito, H. Tsutsui, H. Nambu, M. Anada and S. Hashimoto, *Adv. Synth. Catal.*, 2005, **347**, 1483–1487.
46 T. Takahashi, H. Tsutsui, M. Tamura, S. Kitagaki, M. Nakajima and S. Hashimoto, *Chem. Commun.*, 2001, 1604–1605.
47 T. Han, Y. Zhang, Q. Cao, S. Liu, Z. Chi and J. Xu, *Polym. Adv. Technol.*, 2013, **24**, 807–813.
48 J. Liu, C. Fasel, P. Braga-Groszewicz, N. Rothermel, A. S. L. Thankamony, G. Sauer, Y. Xu, T. Gutmann and G. Buntkowsky, *Catal. Sci. Technol.*, 2016, **6**, 7830–7840.

49 J. Liu, Y. Xu, P. B. Groszewicz, M. Brodrecht, C. Fasel, K. Hofmann, X. Tan, T. Gutmann and G. Buntkowsky, *Catal. Sci. Technol.*, 2018, **8**, 5190–5200.
50 G. Nickerl, U. Stoeck, U. Burkhardt, I. Senkovska and S. Kaskel, *J. Mater. Chem. A*, 2014, **2**, 144–148.
51 A. Awata and T. Arai, *Synlett*, 2013, **24**, 29–32.
52 Y. Chi, L. Qiu and X. Xu, *Org. Biomol. Chem.*, 2016, **14**, 10357–10361.
53 T. Hirayama, A. Kumar, K. Takada and T. Kaneko, *ACS Omega*, 2020, **5**, 2187–2195.
54 S. Mallakpour and H. Ayatollahi, *J. Thermoplast. Compos. Mater.*, 2015, **28**, 3–18.
55 C. G. Espino, K. W. Fiori, M. Kim and J. Du Bois, *J. Am. Chem. Soc.*, 2004, **126**, 15378–15379.
56 E. B. Boyar and S. D. Robinson, *Coord. Chem. Rev.*, 1983, **50**, 109–208.
57 K. Sanada, H. Ube and M. Shionoya, *J. Am. Chem. Soc.*, 2016, **138**, 2945–2948.
58 J. Long, G. Liu, T. Cheng, H. Yao, Q. Qian, J. Zhuang, F. Gao and H. Li, *J. Catal.*, 2013, **298**, 41–50.
59 G. Kumari, M. Modi, S. K. Gupta and R. K. Singh, *Eur. J. Med. Chem.*, 2011, **46**, 1181–1188.
60 M. Palomba, L. Rossi, L. Sancineto, E. Tramontano, A. Corona, L. Bagnoli, C. Santi, C. Pannecouque, O. Tabarrini and F. Marini, *Org. Biomol. Chem.*, 2016, **14**, 2015–2024.
61 P. B. Sampson, Y. Liu, B. Forrest, G. Cumming, S.-W. Li, N. K. Patel, L. Edwards, R. Laufer, M. Feher and F. Ban, *J. Med. Chem.*, 2015, **58**, 147–169.
62 B. Yu, Z. Yu, P.-P. Qi, D.-Q. Yu and H.-M. Liu, *Eur. J. Med. Chem.*, 2015, **95**, 35–40.

